Superconductor Science and Technology

PAPER • **OPEN ACCESS**

Effects of K excess in microstructure of $(Ba_{0.6}K_{0.4})Fe_2As_2$ superconducting powders

To cite this article: Emilio Bellingeri *et al* 2024 *Supercond. Sci. Technol.* **37** 095014

OPEN ACCESS
IOP Publishing
Superconductor Science and Technology
Supercond. Sci. Technol. **37** (2024) 095014 (9pp)
https://doi.org/10.1088/1361-6668/ad68d4

Effects of K excess in microstructure of $(Ba_{0.6}K_{0.4})Fe_2As_2$ superconducting powders

Emilio Bellingeri[1,*], Cristina Bernini[1], Federico Loria[1], Andrea Traverso[1], Alessandro Leveratto[1], Valeria Braccini[1], Amalia Ballarino[2] and Andrea Malagoli[1]

[1] CNR-SPIN, Corso Perrone 24, 16152 Genova, Italy
[2] European Organisation for Nuclear Research (CERN), Geneva, Switzerland

E-mail: emilio.bellingeri@spin.cnr.it

Received 30 May 2024, revised 18 July 2024
Accepted for publication 29 July 2024
Published 14 August 2024

Abstract

Iron-based superconductors (IBSs) are promising for high-field applications due to their exceptional characteristics, like ultrahigh upper critical field and minimal electromagnetic anisotropy. Creating multifilamentary superconducting wires with elevated transport critical current density is essential for practical use. The Powder in Tube (PIT) technique is commonly used for this purpose, but achieving optimal results requires careful exploration of powder microstructural properties. This is particularly crucial for superconductors like (Ba,K)122, the IBS most promising from an applicative point of view, where factors such as reactivity, volatility, and toxicity of constituent elements affect phase formation. Potassium volatility often leads to nonstoichiometric conditions, introducing excess potassium in the formulation. This study focuses on the impact of potassium excess δ on the microstructural properties of the 'optimally doped' $(Ba_{0.6}K_{0.4+\delta})Fe_2As_2$ phase ($0 \leqslant \delta \leqslant 0.08$). Using techniques like Scanning Electron Microscopy, x-ray diffraction, and temperature-dependent magnetization measurements, we demonstrate the ability to produce nearly pure powders of the superconducting phase with controlled grain size. Our findings are relevant for PIT wire fabrication, where grain size strongly affects mechanical deformation. Grain size also influences transport properties, as observed in previous studies, where reducing grain size enhanced current-carrying capability at high magnetic fields.

Keywords: microstructure, (Ba0.6K0.4)Fe2As2, iron based superconductors, K excess

1. Introduction

In recent years, iron-based superconductors (IBSs) have garnered significant attention within the international superconducting community. Unlike traditional low-temperature superconductors, IBS materials exhibit compelling advantages, including higher upper critical fields, enhanced critical current densities (J_c), elevated transition temperatures T_c [1] while compared to copper oxide HTS counterparts, reduced anisotropy, wider critical angles, and improved grain boundary connectivity [2]. These properties position IBSs as promising candidates for practical applications across a broad range of medium- to high-temperature and high-field scenarios [3].

Among the IBS materials, the (Ba,K)122 compound has emerged as a focal family due to its intriguing properties. Notably, the successful preparation of a 100-meter-long

* Author to whom any correspondence should be addressed.

$Sr_{1-x}K_xFe_2As_2$ (Sr-122) IBS wire realized by the Powder-In-Tube (PIT) method in 2016 demonstrated the feasibility of large-scale production [4]. Furthermore, (Ba,K)122 PIT samples achieved transport J_c as high as 1.5×10^5 A cm^{-2} in tapes [5] and 4.4×10^4 A cm^{-2} in round wires annealed at ambient pressure at 4.2 K and 10 T [6, 7]. These milestones underscore the practical viability of IBSs [8].

Despite these achievements, the development of (Ba,K)122 IBS wires and tapes faces hurdles. Issues related to processing stability and formability persist. Other technologically advanced HTS PIT wires and tapes, such as Bi-based ones, have benefited from comprehensive characterization efforts on their development path. Among them powerful techniques such as in situ monitoring using synchrotron x-ray or neutron diffraction have shed light on reaction dynamics within the wire and additionally, extensive experimental and theoretical investigations have elucidated the mechanical behavior during processing, paving the way for the development of superconducting wires and tapes with more than 100 cores [9–11]. A similar approach would be extremely important to define the process parameters also for (Ba,K)122 wire fabrication and, finally, establish the actual potential of this superconductor in applications such as high field magnets.

In general, concerning the PIT method, a crucial aspect regards the morphological and superconducting characteristics of the precursor powders and thus the parameters of the process used to obtain them. The optimization route to get a high-performance superconducting wire passes necessarily through the tuning of parameters such as high purity precursors, heat treatment, purity and cleanliness of the grain boundaries which have to guarantee transport properties as good as possible, and granulometry, that must allow a suitable powder particles flow during the cold deformation [12–15].

In this context, the presence of excess potassium beyond the intended stoichiometric ratio emerges as a pivotal determinant for achieving optimal superconducting properties in the synthesis of (Ba,K)122. Potassium supplementation is frequently noted in literature as indispensable to counterbalance the losses of this volatile element during the phase formation process. Nonetheless, the intricate nature of synthesis procedures under conventional conditions has limited comprehensive investigations into this phenomenon. Notably, a prior investigation [16] revealed that the function of surplus potassium extends beyond mere compensation for losses.

In this study, we introduce a novel powder synthesis technique that effectively mitigates elemental losses, allowing us to elucidate the multifaceted impact of excess potassium on the synthesis and microstructural characteristics of (Ba,K)122 powders. Our findings demonstrate that the incorporation of potassium exerts a favorable influence on rapid growth and crystallization rates, while also affording control over grain size variation. Remarkably, the manipulation of potassium dosage facilitates the production of powders with diverse grain sizes. This precise control over particle dimensions holds paramount significance, both in the mechanical deformation processes involved in multifilament conductor preparation and in optimizing critical current values for conductors characterized by low texture, such as wires exhibiting high shape isotropy [17].

2. Method

A homogeneous set of samples was prepared by varying the K excess δ in the 'optimally doped' (Ba0.6K0.4 + δ)Fe2As2 phase in the range $0 \leqslant \delta \leqslant 0.08$, corresponding to up to 20% excess K. The phase was synthesized from a stoichiometric mixture (plus the desired K excess) of pure metallic elements: Fe 99.99% powder; K 99.99% solid; Ba 99.25% (+ 0.75%Sr) and As 99.99% chunks. The elements were mixed using an NSE Supplies LLC Model PMV1GB-0.2 l planetary ball milling machine for 10 h to achieve a highly homogeneous mixture, ensuring high element dispersion uniformity and obtaining a highly reactive powder.

Yttria stabilized zirconia YSZ jars and spherical milling media were employed, with a ball-to-precursor mass ratio of 10:1. The milling media consisted of ball diameters of $d1 = 0.8$ mm and $d2 = 0.5$ mm, with a diameter distribution ratio of $\#d1/\#d2 = 0.4$. Based on the transferred energy calculation from [18], the energy at the employed rotational speed of 750 RPM for all the samples was evaluated to be 18.6 MJ kg^{-1}. No contamination attributable to the milling process was detected by Scanning Electron Microscopy (SEM) or XRD analysis. The powder obtained was enclosed in a Nb envelope and then hermetically sealed in an Ar atmosphere in a stainless-steel crucible. The entire process was performed in a glove box with an Ar controlled atmosphere containing less than 0.5 ppm of O_2 and 0.5 ppm of moisture. The powder/crucible ratio was kept constant for all the tests described here. The crucible was finally heated at 870 °C for 20 h while continuously rotating off-axis by about 40 mm to optimize the mixing of elements during the reaction. The produced powder remained stable in air and was gently grounded in an agate mortar. A portion of the powder was mixed with a Si powder standard for XRD measurement using the Malvern Panalytical X'pert PRO with X'Celeretor detector to refine the cell parameters precisely; night long measurements were employed to refine phase content and atoms occupation. The microstructure of the synthesized powders was examined using Leica Cambridge Scanning Electron Microscope S 360. To facilitate grain counting and assess grain size, the powders were gently pressed in pellets, ensuring a suitable planar surface. For grain size evaluation, 5 SEM images were sampled from various regions of each sample. These images were acquired at different magnifications, aiming for a consistent grain count in each image. Subsequently, a Matlab routine was employed to determine the grain diameters d by analyzing the diameters of grains in each image; a detailed description of the procedure is reported in [19]. Particle diameters were statistically analyzed to provide a frequency count as a function of diameter. Each distribution was finally fitted with a lognormal curve.

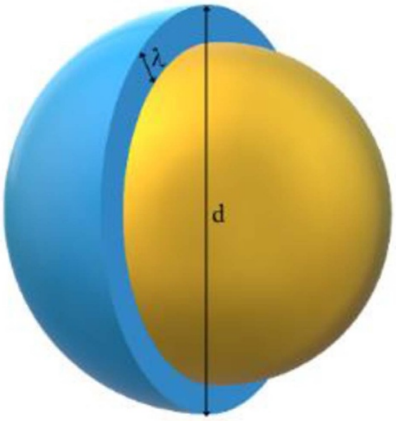

Figure 1. Schematic view of the effective screened region contributing to the FC magnetization due to the London penetration depth.

The magnetization of the ground powders was measured using a Quantum Design DC SQUID. The experimental magnetization curve versus temperature at 10 G, depicting the transition from the normal state to the superconducting state, was measured for all the powders.

In the case of grain powder of a small size, it is necessary to take into account the London penetration depth effect when analyzing the magnetization data. Similar to the method described in [19], we estimate the contribution to volume magnetization by considering the volume of a grain that is effectively shielded from the magnetic field as sketched in figure 1.

This quantity varies with temperature, following the temperature dependence of the London penetration depth as outlined by Ginzburg–Landau theory.

$$\lambda(T) = \frac{\lambda_0}{\sqrt{1-\left(\frac{T}{T_c}\right)^n}}.$$

The power index n in the $\lambda(T)$ analytical expression reflects different mechanisms: $n = 4$ for strong coupling, $n = 3$ for weak coupling, and $n = 2$ for unconventional pairing states with high impurity levels. For the (Ba,K)122 family, n varies between 1.8 and 2.6 [20], and the initial penetration depth (λ_0) depends on doping levels, typically reported around 200 nm for optimally doped materials [21].

The magnetization of a single grain below T_c, following the approximation in [19] can thus be written as:

$$m(t) = \left(1 - \frac{2\lambda(T)}{x}\right)^3.$$

In contrast to our approach in [18], where only the average grain size was considered, the present study accounts for the entire grain size distribution due to the broader distribution of particle sizes, so the $M(T)$ sample magnetization can be calculated integrating over x on the normalized grain distribution $f(x)$:

$$M(T) = K\int_0^\infty f(x)\, m(T,x)\, \mathrm{d}x.$$

So in our case, for a lognormal distribution

$$f(x) = \frac{1}{x\sigma\sqrt{2\pi}} e^{-\left(\frac{lnx-\mu}{2\sigma}\right)^2}.$$

The magnetization at temperature T can be calculated as

$$M_{Teo}(T) = K\int_0^\infty \frac{1}{x\sigma\sqrt{2\pi}} \mathrm{e}^{-\left(\frac{lnx-\mu}{2\sigma}\right)^2} \left(1 - \frac{2\lambda(T)}{x}\right)^3 \mathrm{d}x.$$

This curve was employed to fit experimental FC magnetization measurements using T_c and the σ and μ parameter of the LogNormal distribution. The integral in the $M_{Teo}(T)$ expression was numerically evaluated up to a 95% quantile. The quantity $\chi^2 = \sum_i \left(M_{Teo}(T_i) - M_{\mathrm{Exp}}(T_i)\right)^2$ was minimized adopting a nonlinear Generalized Reduced Gradient.

3. Results and discussion

The diffraction spectrum illustrating samples with potassium excess ranging from 0%–20% is presented in figure 2. The peaks corresponding to the $(Ba_{0.6}K_{0.4})Fe_2As_2$ phase are indexed ; '*' denoted the primary Fe metal peak and '+' denoted one of the more intense peaks of the Fe_2As phase. The figure reveals that only a nominal presence of impurities is observed for samples with low or no excess potassium. For potassium excess up to 15%, traces of crystalline metallic Fe (<1%) are discernible, while solely the peaks associated with the superconducting phase are evident at a potassium excess of 20%.

Utilizing Rietveld refinements, the potassium-to-barium ratio in the phase was estimated, and the results are depicted in figure 3(a). The obtained value aligns with expectations, albeit slightly higher than the one anticipated (Ba:K == 0.6:0.4).

Intriguingly, a diminishing trend in potassium content is observed as the initial stoichiometric excess of potassium increases. However, the precision of this measurement introduces uncertainty, precluding a definitive confirmation of this trend. To validate these findings, XRD measurements were performed using a silicon standard, enabling the refinement of phase cell parameters with exceptional precision. The refined values are tabulated in table 1 and plotted in figure 3(b). From these data, particularly the c-axis value, a comparison with literature data [22], suggests that, under the assumption that variations depend solely on the stoichiometric ratio Ba:K, it is possible to estimate this ratio. This estimation is also illustrated in figure 2. Even with these assumptions, the estimate supports the tendency of potassium to decrease marginally as the excess potassium in the initial stoichiometry rises. The behavior of the a cell parameter, that increases with the K excess, again supports this information. However, our results contrast with [16], where the potassium content initially increased based on the

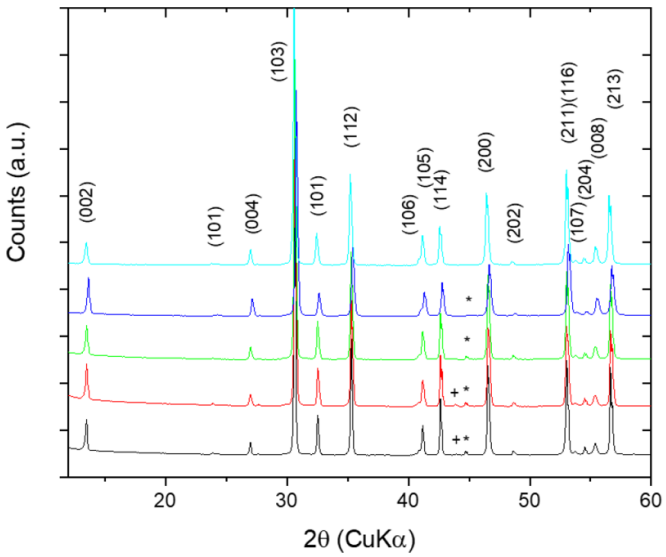

Figure 2. XRD spectra of (Ba,K)122 samples prepared with different K excess (0, 5, 10, 15, 20% from bottom to top, respectively). The peaks corresponding to the (Ba0.6K0.4)Fe2As2 phase are indexed. * is the primary Fe metal peak and + is one of the more intense peaks of the Fe2As phase.

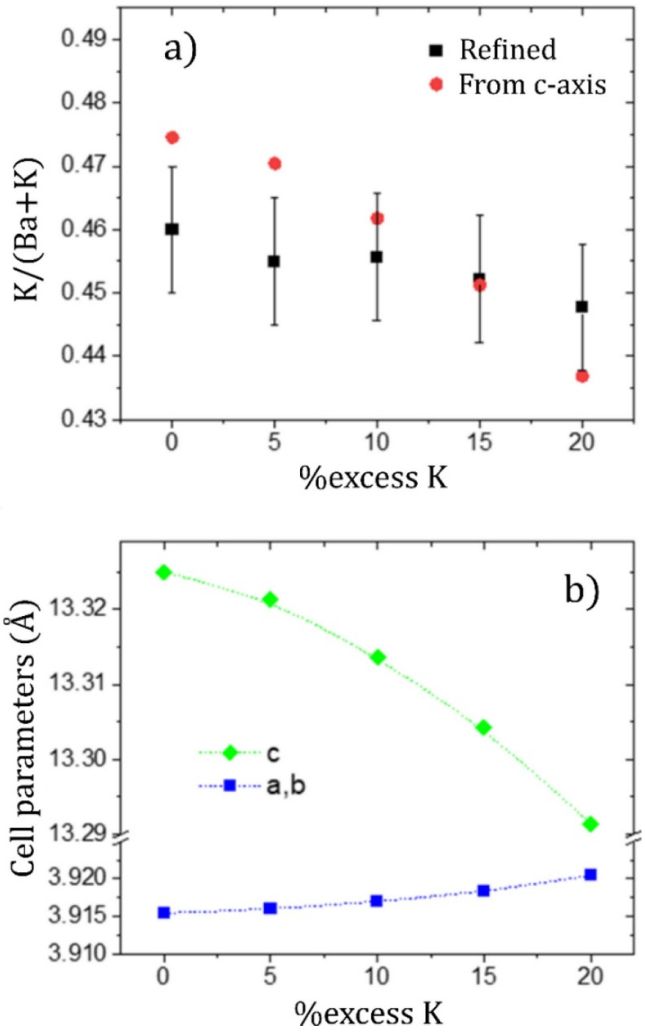

Figure 3. (a) Refined and calculated from [22] K occupancy in Ba,K site vs K excess and b) refined cell parameter.

Table 1. Structural parameters values obtained through Rietveld refinements.

K %	Ba(122) %	Fe %	a,b Å	C Å	K/(K + Ba)
0	95	3	3.91542(2)	13.3251(1)	0.461(5)
5	96	1	3.91599(2)	13.3213(1)	0.455(5)
10	98	1,5	3.91696(2)	13.3136(1)	0.455(6)
15	100	—	3.91828(2)	13.3042(1)	0.452(5)
20	100	—	3.92052(2)	13.2914(1)	0.447(5)

Table 2. Chemical composition (in atomic percentage) of the (Ba,K)122 phase in the samples prepared with different K excess (0, 5, 10, 15, 20%) analyzed through EDS spectroscopy (EHT = 20 KV).

Excess K % (weight)	K % (atomic)	Fe % (atomic)	As % (atomic)	Ba % (atomic)
0	8.7 ± 1.4	40.0 ± 0.4	39.0 ± 0.5	12.2 ± 1.7
5	8.7 ± 0.4	40.0 ± 0.7	39.0 ± 0.6	12.3 ± 0.6
10	8.5 ± 0.6	40.0 ± 1.4	38.4 ± 1.3	13.2 ± 0.6
15	8.2 ± 0.1	40.1 ± 0.4	38.7 ± 0.5	13.0 ± 0.2
20	8.0 ± 0.5	39.9 ± 0.5	38.6 ± 1.0	13.6 ± 0.2

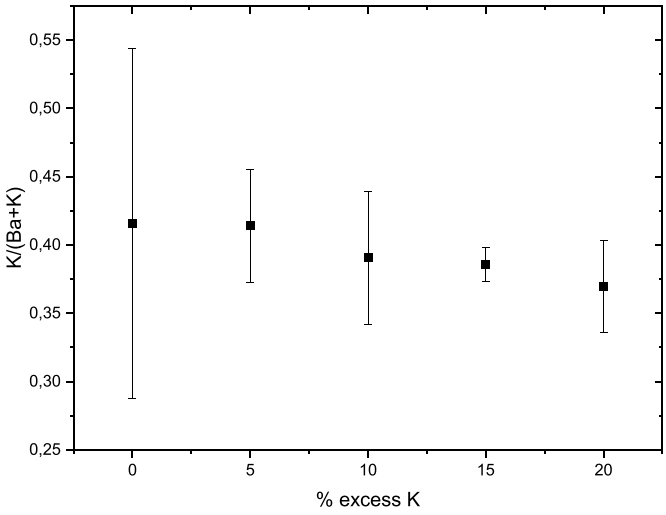

Figure 4. K/K + Ba ratio of the (Ba,K)122 phase within the powder grains as a function of the initial potassium excess.

initial amount. This discrepancy can be explained by the detection of small potassium losses in their preparation process.

Using the Oxford X-Max 20 Energy-Dispersive Spectrometer, housed within the SEM, pellets prepared from various powder samples with different potassium excess percentages were analyzed to evaluate their chemical composition. The results of the semi-quantitative analyses, provided by the dedicated Oxford Aztec 4.2 Software and conducted globally on all the entire pellets, unveiled a higher actual potassium content in the samples synthesized with potassium excess. This indicates the effectiveness of our powder synthesis process in minimizing elemental losses and enables us to investigate the influence of excess potassium on the microstructural properties of (Ba,K)122 powders.

Overall, the powders appear to be pure, predominantly composed of the (Ba,K)122 phase, with occasional impurities of Fe and very rare occurrences of Fe–As compound, particularly noticeable in samples with lower potassium excess. For each (Ba,K)122 sample, encompassing various potassium excess percentages, we conducted EDS analysis of multiple grains constituting the resulting phase reporting both the average compositional values and the standard deviation of their distribution for each compositional element (see table 2).

The (Ba,K)122 phase observed exhibits varying potassium-to-barium ratios ranging from Ba:K 0.63:0.37 to Ba:K 0.58:0.42 (assuming the full occupancy of the Ba site, as confirmed by the Rietveld XRD refinement) as confiacross the different samples.

Figure 4 Illustrates the potassium-to-barium ratio within the phase as a function of the initial stoichiometric excess of potassium in the samples. A trend of decreasing potassium content with increasing initial stoichiometric excess of potassium is observed. This trend mirrors the observations made through Rietveld refinements in x-ray Diffraction measurements. However, slightly higher potassium content values are observed in all phases obtained from EDS analyses, possibly due to experimental measurement limitations. EDS mappings (figure 5) performed on the various samples enabled us to analyze the elemental distribution within the powders and evaluate their uniformity. In samples with a K excess of 15% and 20%, alongside the (Ba,K)122 phase, we identified grains of free potassium, clearly visible in the color map in figure 5(a), where yellow corresponds to K. On the contrary, for K excess of 10%, 5% and 0% we observe a homogeneous distribution of potassium with no evidence of accumulation among the grains (figure 5(b)). Moreover, in certain instances, we observed potassium bound to niobium, a component of the crucible, which tends to react with the excess potassium during powder synthesis.

This phenomenon elucidates the stoichiometric compensation and confirms the absence of potassium losses during the synthesis step. The grain size distribution obtained through SEM analysis, along with a representative image used for calculating the distribution, is presented in figure 6. The data for all samples conform closely to a lognormal distribution, indicating its suitability for describing the grain size variations. Notably, the grain size demonstrates a significant dependence on the K excess in the samples. From the parameters of the lognormal fitting (denoted as m and s), the average grain size ($\bar{d}$) can be calculated using the formula $\bar{d} = e^{\mu + \frac{\sigma^2}{2}}$.

For instance, the average grain size is found to be 1.6 μm for the stoichiometric compound and increases to 8.3 μm for the sample with a 20% K excess. These mean grain size values, along with the full width at half maximum of the distribution, are summarized in panels b and a of figure 7, respectively. Additionally, results derived from the m and s values obtained from the above described fitting procedure of the ZFC (Zero

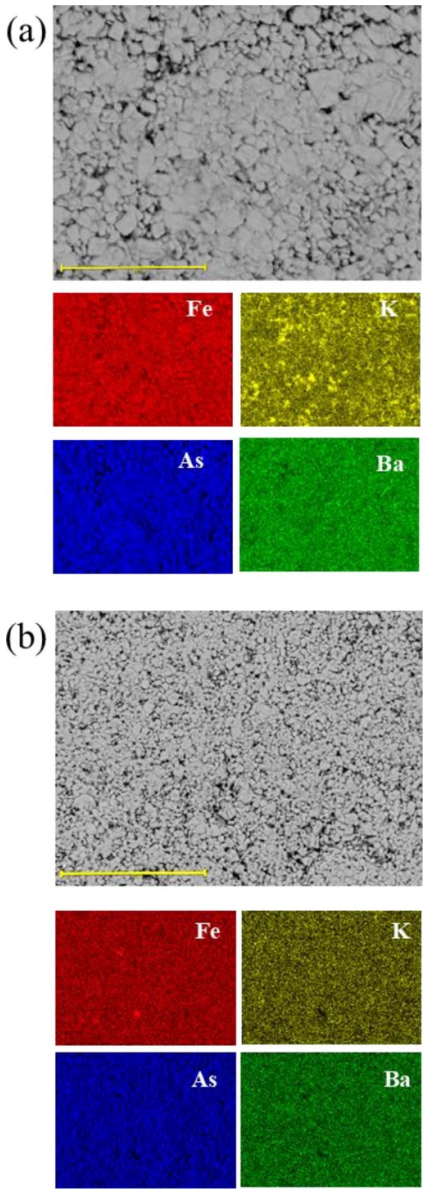

Figure 5. EDS elemental mapping of (Ba,K)122 samples prepared with two different K excess; (a) 20% and (b) 10%. Scale bars: 50 μm.

Field Cooling) magnetization curves (reported in figure 8) are also provided.

It is worth noting that despite differences in methodology and the assumed parameters in the $M(T)$ curves, the values obtained exhibit reasonable agreement.

Moreover, the fitting of the $M(T)$ curves, assuming an ideal diamagnetic response for bulk superconductors, attributes the broadening of the curve primarily to the small grain size of the powder.

This observation together with the fact that, the variation in the superconducting critical temperature (T_c) remains minimal ($<$1 K) across all samples around $T_c = 38$ K, consistently with the literature's best-reported values, underscores the high-quality superconducting behavior exhibited by all the samples.

The proposed method for the (Ba,K)122 superconducting powders allows the preparation of almost pure phase in all the conditions explored. The excess of K in the formula is beneficial for the grain growth and marginally for the phase purity but, at the same time does not enter into the final phase, This effect can be partly explained by considering that at the highest temperature during the heat treatment (950 °C), a significant portion of the potassium may be in the gaseous state, leading to a lower local concentration of potassium at the grain edges where the phase tends to grow. Excess potassium mitigates this phenomenon by increasing the partial pressure of potassium, thereby enhancing its availability during phase formation and grain growth from precursors in the solid/liquid phase. This promotes phase formation and improves purity, resulting in a significant reduction of secondary phases (such as Fe and

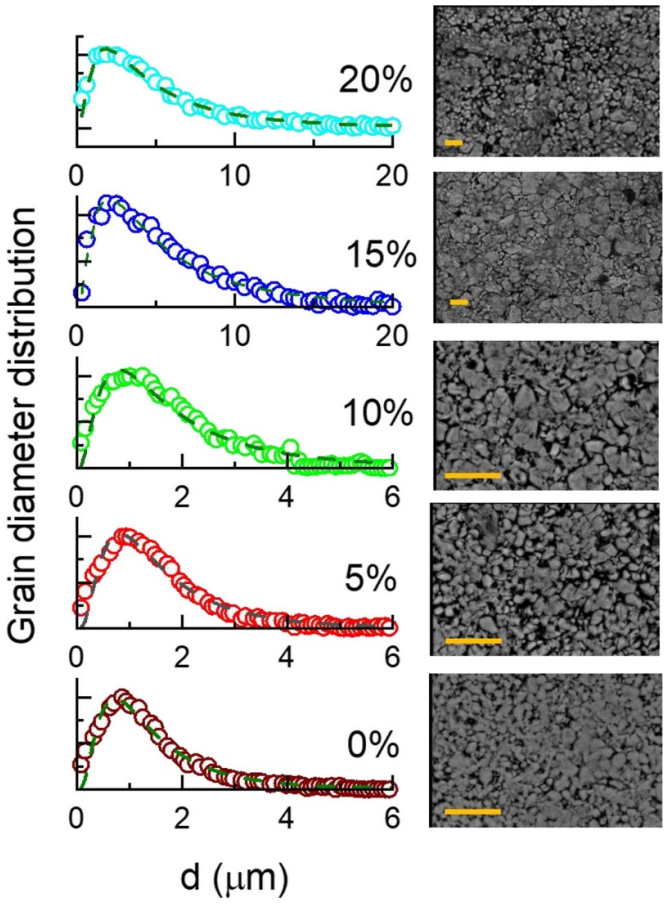

Figure 6. Grain size distribution and lognormal fit (left) obtained from SEM images (right) for samples prepared with different K excess. The marker in the SEM micrography correspond to 10 μm. Note that the first two image (20 and 15%) has a different magnification adopted to get images with a comparable number of grains on which to proceed with the calculation of the grain size distribution.

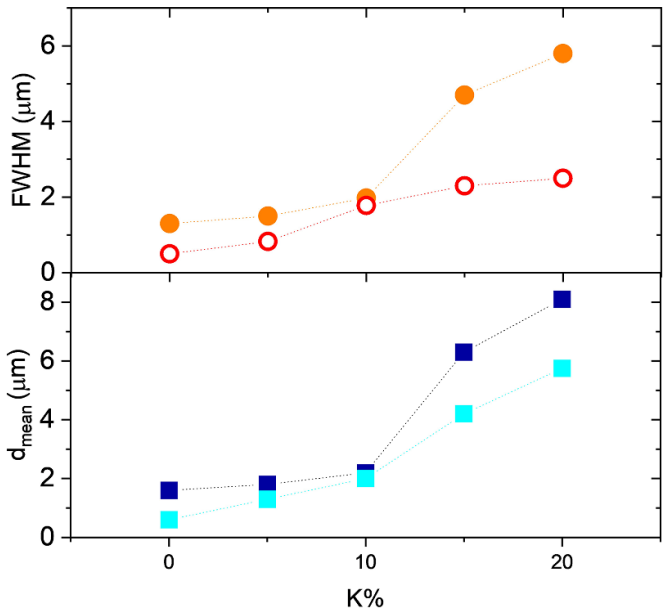

Figure 7. Average grain size (a) and width of its distribution (b) as a function of K excess obtained by the SEM analysis (filled symbols) and from the FC magnetization fit (hollowed symbols).

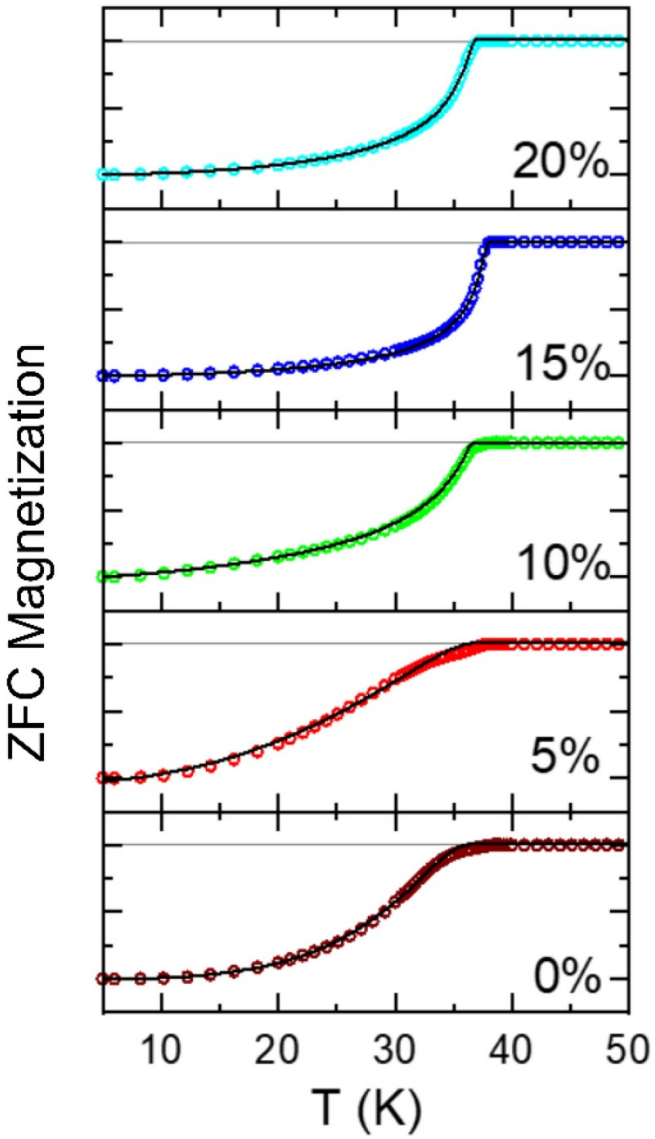

Figure 8. ZFC magnetization curves vs temperature measured by DC SQUID at 10 Gauss for samples prepared with different K excess. The experimental data (symbols) are fitted by theoretical curves (lines) obtained considering the Ginzburg-Landau temperature dependance of the London penetration depth.

FeAs2) after the reaction. Additionally, we observe that excess potassium facilitates the formation of a phase with a Ba/K ratio that brings the Fe–As angle closer to the ideal tetrahedral angle of approximately 109° [22]. Consequently, excess potassium is favorable for the formation of the Ba(122) phase in its more thermodynamically and crystallographic stable structure.

4. Conclusions

Our analysis of grain size distribution using SEM revealed a close adherence to a lognormal distribution across all samples, indicating its suitability for describing grain size variations. The dependence of grain size on potassium excess was pronounced, with average grain size increasing from 1.6 μm for the stoichiometric compound to 8.3 μm for samples with a 20% K excess. Additionally, the parameters derived from fitting the field cooling magnetization curves showed reasonable agreement across samples. Attributing broadening primarily to small grain size and considering that, the T_c is always close to 38 K underscores the high-quality superconducting behavior exhibited by all samples.

Our method for preparing (Ba,K)122 superconducting powders consistently yielded nearly pure phase under all explored conditions. The strong point is the innovative use of a rotating furnace which allows an optimal continuous mixing of the precursors during the heat treatment being furthermore a very simple and scalable process.

While excess potassium promoted grain growth, it did not incorporate into the final phase; in fact, samples with higher K excess exhibited slightly lower K/Ba ratios. It is the first time, in our knowledge, that a correlation between the K excess and a significant grain growth has been recorded. These findings highlight the efficacy of our approach for producing high-quality superconducting powders and manipulating and also tuning their morphological characteristics such as the granulometry, a key factor in optimizing PIT processed conductors suitable for applications in various fields.

Data availability statement

All data that support the findings of this study are included within the article (and any supplementary files).

Funding statement

The financial support through The Addendum N.3 KE5814/TE to The Memorandum Of Cooperation For The High field Magnet (HFM) Research And Development Programme KN5623 is acknowledged.

ORCID iDs

Emilio Bellingeri https://orcid.org/0000-0001-7902-0706
Andrea Traverso https://orcid.org/0000-0002-9690-2222
Alessandro Leveratto https://orcid.org/0000-0001-8480-2884
Valeria Braccini https://orcid.org/0000-0003-0073-367X
Andrea Malagoli https://orcid.org/0000-0002-7204-9204

References

[1] Togano K, Matsumoto A and Kumakura H 2011 Large transport critical current densities of Ag sheathed (Ba,K)Fe_2As_2+Ag superconducting wires fabricated by an *Ex-situ* powder-in-tube process *Appl. Phys. Express* **4** 043101
[2] Putti M *et al* 2010 New Fe-based superconductors: properties relevant for applications *Supercond. Sci. Technol.* **23** 034003
[3] Yao C and Ma Y 2021 Superconducting materials: challenges and opportunities for large-scale applications *iScience* **24** 102541
[4] Ma Y 2012 Progress in wire fabrication of iron-based superconductors *Supercond. Sci. Technol.* **25** 113001

[5] Huang H, Yao C, Dong C, Zhang X, Wang D, Cheng Z, Li J, Awaji S, Wen H and Ma Y 2018 High transport current superconductivity in powder-in-tube $Ba_{0.6}K_{0.4}Fe_2As_2$ tapes at 27 T *Supercond. Sci. Technol.* **31** 015017

[6] Guo W, Yao C, Xiong H, Yang P, Tu C and Ma Y 2024 High transport J_c performance by enhancing grain coupling in (Ba,K)Fe_2As_2 multi-filamentary wires *Sci. China Mater.* **67** 301

[7] Fu C, Dong C, Tu C, Han M, Huang H, Wang D, Zhang X and Ma Y 2024 High critical current density in low-cost iron-based superconducting round wires annealed at ambient pressure *Supercond. Sci. Technol.* **37** 035015

[8] Yao C and Ma Y 2019 Recent breakthrough development in iron-based superconducting wires for practical applications *Supercond. Sci. Technol.* **32** 023002

[9] Malagoli A, Lee P, Ghosh A, Scheuerlein C, Di Michiel M, Jiang J, Trociewitz U, Hellstrom E and Larbalestier D 2013 Evidence for length-dependent wire expansion, filament dedensification and consequent degradation of critical current density in Ag-alloy sheathed Bi-2212 wires *Supercond. Sci. Technol.* **26** 055018

[10] Martinelli A, Bellingeri E, Leveratto A, Leoncino L, Ritter C and Malagoli A 2018 *Phys. Rev. Mater.* **2** 084801

[11] Giannini E, Bellingeri E, Passerini R and Flükiger R 1999 Direct observation of the Bi,Pb(2223) phase formation inside Ag-sheathed tapes and quantitative secondary phase analysis by means of in situ high-temperature neutron diffraction *Physica* C **315** 185

[12] Pak C, Su Y F, Tarantini C, Hellstrom E E, Larbalestier D C and Kametani F 2020 Synthesis routes to eliminate oxide impurity segregation and their influence on intergrain connectivity in K-doped $BaFe_2As_2$ polycrystalline bulks *Supercond. Sci. Technol.* **33** 084010

[13] Kametani F, Su Y-F, Collantes Y, Pak C, Tarantini C, Larbalestier D and Hellstrom E 2020 Chemically degraded grain boundaries in fine-grain $Ba_{0.6}K_{0.4}Fe_2As_2$ polycrystalline bulks *Appl. Phys. Express* **13** 113002

[14] Tarantini C, Pak C, Su Y F, Hellstrom E E, Larbalestier D C and Kametani F 2021 Effect of heat treatments on superconducting properties and connectivity in K-doped $BaFe_2As_2$ *Sci. Rep.* **11** 3143

[15] Chen Y, Li W, Liu C, Huang H, Yao C, Zhang X, Wang D, Liu F, Liu H and Ma Y 2022 Effects of precursor powder particle size on the powder-in-tube $Ba_{1-x}K_xFe_2As_2$ superconducting tapes *Supercond. Sci. Technol.* **35** 055008

[16] Wang C, Wang L, Gao Z, Yao C, Wang D, Qi Y, Zhang C and Ma Y 2011 Enhanced critical current properties in $Ba_{0.6}K_{0.4+x}Fe_2As_2$ superconductor by over-doping of potassium *Appl. Phys. Lett.* **98** 042508

[17] Hecher J, Baumgartner T, Weiss J D, Tarantini C, Yamamoto A, Jiang J, Hellstrom E E, Larbalestier D and Eisterer M 2015 Small grains: a key to high-field applications of granular Ba-122 superconductors? *Supercond. Sci. Technol.* **29** 025004

[18] Häßler W, Hermann H, Herrmann M, Rodig C, Aubele A, Schmolinga L, Sailer B and Holzapfel B 2013 Influence of the milling energy transferred to the precursor powder on the microstructure and the superconducting properties of MgB2 wires *Supercond. Sci. Technol.* **26** 025005

[19] Vignolo M, Bovone G, Bellingeri E, Bernini C, Romano G, Buscaglia M T, Buscaglia V and Siri A S 2014 Size determination of superconducting MgB_2 powder from magnetization curve, image analysis and surface area measurements *Supercond. Sci. Technol.* **27** 065007

[20] Prozorov R and Kogan V G 2011 London penetration depth in iron-based superconductors *Rep. Prog. Phys.* **74** 124505

[21] Lee S, Seo Y S, Roh S, Song D, Eisaki H and Hwang J 2022 Doping-dependent superconducting physical quantities of K-doped $BaFe_2As_2$ obtained through infrared spectroscopy *Sci. Rep.* **12** 19950

[22] Avci S *et al* 2012 Phase diagram of Ba_{1-x} $K_xFe_2As_2$ *Phys. Rev.* B **85** 184507